

## Photo-Thermo Catalysis

Zitierweise: *Angew. Chem. Int. Ed.* **2020**, 59, 12909–12916

Internationale Ausgabe: doi.org/10.1002/anie.202001701

Deutsche Ausgabe: doi.org/10.1002/ange.202001701

# Photo-thermo Catalytic Oxidation over a TiO<sub>2</sub>-WO<sub>3</sub>-Supported Platinum Catalyst

Leilei Kang, Xiao Yan Liu,\* Aiqin Wang, Lin Li, Yujing Ren, Xiaoyu Li, Xiaoli Pan, Yuanyuan Li, Xu Zong, Hua Liu, Anatoly I. Frenkel und Tao Zhang\*

**Abstract:** Photo-thermo catalysis, which integrates photocatalysis on semiconductors with thermocatalysis on supported nonplasmonic metals, has emerged as an attractive approach to improve catalytic performance. However, an understanding of the mechanisms in operation is missing from both the thermo- and photocatalytic perspectives. Deep insights into photo-thermo catalysis are achieved via the catalytic oxidation of propane (C<sub>3</sub>H<sub>8</sub>) over a Pt/TiO<sub>2</sub>-WO<sub>3</sub> catalyst that severely suffers from oxygen poisoning at high O<sub>2</sub>/C<sub>3</sub>H<sub>8</sub> ratios. After introducing UV/Vis light, the reaction temperature required to achieve 70% conversion of C<sub>3</sub>H<sub>8</sub> lowers to a record-breaking 90°C from 324°C and the apparent activation energy drops from 130 kJ mol<sup>-1</sup> to 11 kJ mol<sup>-1</sup>. Furthermore, the reaction order of O<sub>2</sub> is -1.4 in dark but reverses to 0.1 under light, thereby suppressing oxygen poisoning of the Pt catalyst. An underlying mechanism is proposed based on direct evidence of the in-situ-captured reaction intermediates.

## Introduction

Photo- and thermocatalysis have developed separately with their own principles. Meanwhile, the integration of photogenerated charge carriers with thermocatalysis—namely photo-thermo catalysis—is a burgeoning field in its own right.<sup>[1]</sup> It is distinguished from the photothermal reaction,

which merely emphasizes the photoinduced heating effect on reactions.<sup>[2]</sup> The remarkable advantages associated with coupling photonic and thermal stimuli over plasmonic metals (Au, Ag, and Cu) have been studied intensively in many typical reactions.<sup>[3]</sup> By contrast, an in-depth understanding of the photo-thermo catalysis on semiconductor-supported nonplasmonic metals (Pt, Pd, Rh, and so on) is still lacking from both the thermo- and photocatalytic point of views.

Catalytic oxidation reactions using molecular oxygen as the oxidant are industrially important.<sup>[4]</sup> Supported Pt is one of the most active catalysts for this kind of reaction. Distinct from the CO poisoning in CO oxidation,<sup>[5]</sup> the active Pt sites on the surface of catalysts can be easily poisoned by oxygen in most oxidation reactions.<sup>[6]</sup> For instance, the activity of supported Pt catalysts drops sharply with an increase in O<sub>2</sub>/propane (C<sub>3</sub>H<sub>8</sub>) ratios,<sup>[7]</sup> which is a pervasive problem in supported Pt-group metal (PGM) catalysts for hydrocarbon oxidation.<sup>[8]</sup>

Herein, the photo-thermo catalysis of semiconductor-supported Pt catalyst (Pt/TiO<sub>2</sub>-WO<sub>3</sub>) dramatically enhances the catalytic oxidation of C<sub>3</sub>H<sub>8</sub> at low temperatures and high O<sub>2</sub>/C<sub>3</sub>H<sub>8</sub> ratio (volume ratio: 20). With UV/Vis irradiation the reaction temperature required to achieve 70% C<sub>3</sub>H<sub>8</sub> conversion (*T*<sub>70</sub>) decreases from 324°C to 90°C; correspondingly, the apparent activation energy (*E*<sub>a</sub>) reduces more than 10 times. The reaction order (*n*) of the reactants changes sharply, especially for O<sub>2</sub>, where *n* increases from -1.4 to 0.1; thus, the oxygen poisoning of the Pt catalyst can be overcome. For the first time peroxy carbonate (-OCO<sub>3</sub>) was determined to be the intermediate for this reaction, using in situ diffuse reflectance infrared Fourier transform spectroscopy (DRIFTS) and the superoxide anion (O<sub>2</sub><sup>-</sup>) was determined to be the active oxygen species by in situ electron paramagnetic resonance (EPR) under the photo-thermo reaction process. The origin of the synergistic effect between the photo- and thermocatalysis is proposed. Photoinduced charge carriers promoted by rising temperature were determined to be the most important factors that facilitate the activation and desorption of the adsorbed oxygen on the Pt surface.

## Results and Discussion

The Pt/TiO<sub>2</sub>-WO<sub>3</sub> catalyst was synthesized by an impregnation method. By balancing both the light absorption (UV/Vis spectra are presented in the Supporting Information, Figure S1) and the specific surface area (N<sub>2</sub> adsorption-desorption isotherms are presented in Figure S2) of the



[\*] Dr. L. Kang, Prof. Dr. X. Y. Liu, Prof. Dr. A. Wang, Prof. Dr. L. Li, Dr. Y. Ren, X. Li, X. Pan, H. Liu  
CAS Key Laboratory of Science and Technology on Applied Catalysis  
Dalian Institute of Chemical Physics, Chinese Academy of Sciences  
Dalian 116023 (China)  
E-Mail: xyliu2003@dicp.ac.cn

Dr. Y. Ren, X. Li, H. Liu, Prof. Dr. T. Zhang  
University of Chinese Academy of Sciences  
Beijing 100049 (China)  
E-Mail: taozhang@dicp.ac.cn

Dr. Y. Li, Prof. Dr. A. I. Frenkel  
Materials Science and Chemical Engineering Department  
Stony Brook University  
Stony Brook, NY 11794 (USA)

Prof. Dr. X. Zong, Prof. Dr. T. Zhang  
State Key Laboratory of Catalysis, Dalian Institute of Chemical  
Physics, Chinese Academy of Sciences  
Dalian 116023 (China)

Prof. Dr. A. I. Frenkel  
Chemistry Division, Brookhaven National Laboratory  
Upton, NY 11973 (USA)

 Supporting information and the ORCID identification number(s) for the author(s) of this article can be found under:  
 <https://doi.org/10.1002/anie.202001701>.

different supports,  $\text{TiO}_2\text{-WO}_3$  with a molar ratio of 1:1 was selected as the support of the catalyst. The loading of Pt in the  $\text{Pt/TiO}_2\text{-WO}_3$  catalyst was determined to be 0.48% by inductively coupled plasma atomic emission spectroscopy (ICP-AES). Figure S3a presents scanning transmission electron microscopy (STEM) imagery of the reduced  $\text{Pt/TiO}_2\text{-WO}_3$  catalyst. The size of Pt clusters dispersed on the  $\text{TiO}_2\text{-WO}_3$  support is about 0.8 nm. In the energy-dispersive spectroscopy (EDS) mappings of Pt, W, and Ti elements (Figure S3b), the distribution of Pt is in accordance with that of W rather than Ti; Pt deposits preferentially on the surface of  $\text{WO}_3$  because of improved affinity between Pt and  $\text{WO}_3$ .<sup>[9]</sup> Moreover, the X-ray diffraction (XRD) patterns of the  $\text{TiO}_2\text{-WO}_3$  support are composed of anatase and rutile  $\text{TiO}_2$ , and monoclinic  $\text{WO}_3$ . No obvious diffraction peak associated with Pt crystal is seen, indicating that there are no large Pt nanoparticle in the  $\text{Pt/TiO}_2\text{-WO}_3$  catalyst (Figure S4).

Catalytic testing was carried out at atmospheric pressure in a self-designed continuous flow fixed-bed quartz reactor, which allows all of the feed gas to pass through the catalyst bed. The cross-section of the reactor is profiled in Figure S5. The mass space velocity (S.V.) was  $30000 \text{ mL g}_{\text{cat}}^{-1} \text{ h}^{-1}$ . A wide passband infrared (IR) filter was used in the Xenon lamp to avoid the localized thermal effect of IR light on the surface of the catalyst. Moreover, the temperature of the catalyst bed was measured using a thermocouple in the furnace to ensure that the light-induced heating could be balanced. Prior to reaction, the catalyst was reduced in flowing hydrogen

(10%  $\text{H}_2/\text{He}$ ); metallic Pt is the most active site for  $\text{C}_3\text{H}_8$  oxidation, and thus, this improved the activity of the catalyst (Figure S6).<sup>[10]</sup> In contrast, the activity of the  $\text{TiO}_2\text{-WO}_3$  support is sluggish under the same reaction conditions (Figure S7). Figure 1a shows the light-off curves under light with temperature. Evidently, the activity of the  $\text{Pt/TiO}_2\text{-WO}_3$  enhances with an increase in light intensity. The best performance is achieved when the light intensity is  $1000 \text{ mW cm}^{-2}$ . In this case, the  $T_{70}$  is as low as  $90^\circ\text{C}$ , which is  $234^\circ\text{C}$  lower than that in the dark. Additionally, no obvious hysteresis can be found in the light-off curves of the fresh and used  $\text{Pt/TiO}_2\text{-WO}_3$  catalysts, demonstrating excellent stability (Figure S8).

Deep insight into the origin of the enhancement can be obtained from the Arrhenius plot (Figure 1b). The  $E_a$  of our catalyst is  $130 \text{ kJ mol}^{-1}$  in the dark, while it decreases to  $11 \text{ kJ mol}^{-1}$  under strong light. Such a small  $E_a$  value is beyond the contribution of thermodynamics. For clarity, these results are summarized in Figure 1c. Interestingly, the  $E_a$  value is inversely proportional to the power density of the light ( $I$ ):

$$E_a = 65.3 - 0.054I \quad (1)$$

According to this equation,  $E_a$  can be extrapolated to be  $65.3 \text{ kJ mol}^{-1}$  when the light intensity is infinitely close to zero. Considering that the  $E_a$  value is as high as  $130 \text{ kJ mol}^{-1}$  in the dark (dashed arrow in Figure 1c), we speculate that the mechanism of the photo-thermo catalysis is different from

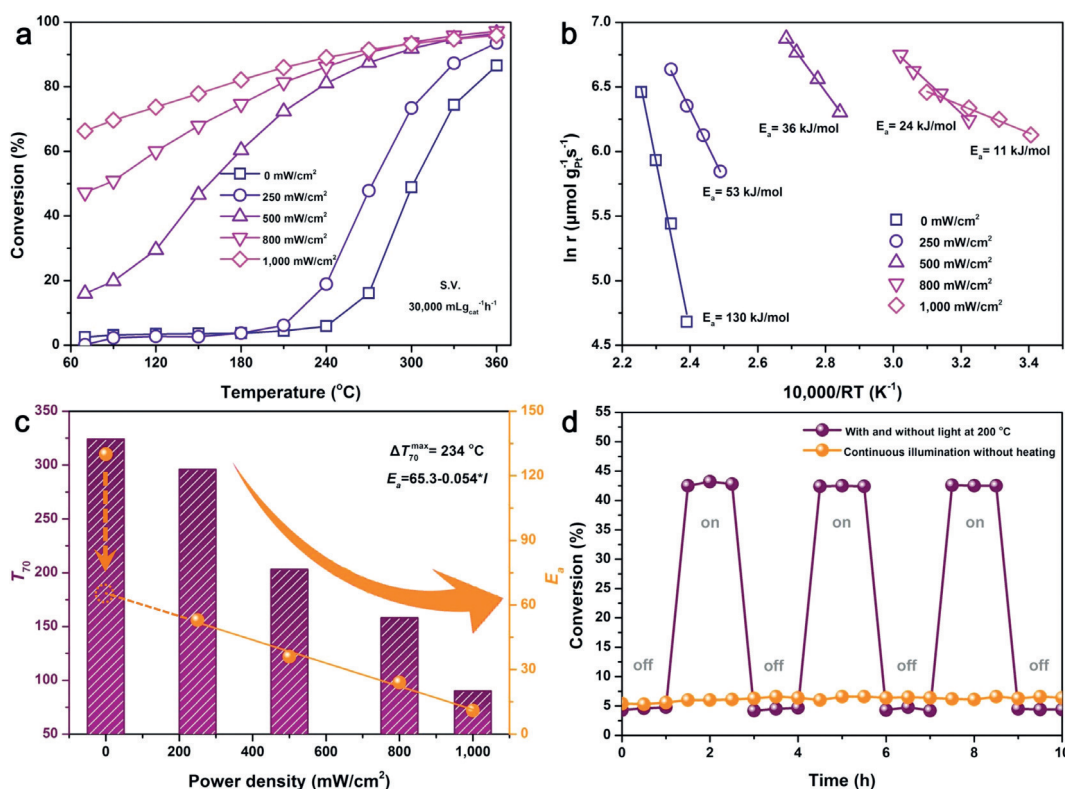


**Figure 1.** a) Catalytic activity, b) Arrhenius plots as well as c)  $T_{70}$  and  $E_a$  of the  $\text{Pt/TiO}_2\text{-WO}_3$  catalyst under light with different power densities. d)  $\text{C}_3\text{H}_8$  conversion on the  $\text{Pt/TiO}_2\text{-WO}_3$  catalyst under continuous illumination without heating and at  $200^\circ\text{C}$  with and without light irradiation (power density:  $400 \text{ mW cm}^{-2}$ ).

that of thermal catalysis. To differentiate the contributions of light and heat, we compared the activities of photocatalysis, thermocatalysis, and photo-thermo catalysis (Figure 1d). Under continuous illumination without heating, the conversion of  $C_3H_8$  is maintained at a mere 5%. We further tracked the steady-state reaction at 200 °C with and without light irradiation. The conversion of  $C_3H_8$  under light (on) surges to approximately 9 times of that in the dark (off). The light-enhancement process is reproducible. Therefore, the superior activity of the Pt/TiO<sub>2</sub>-WO<sub>3</sub> catalyst for catalytic oxidation of  $C_3H_8$  can be attributed to the synergistic effect of light and heat. Furthermore, the specific reaction rates based on the Pt content under different conditions were calculated and compared (Supporting Information, Table S1). For the Pt/TiO<sub>2</sub>-WO<sub>3</sub> catalyst, the specific reaction rate of 457.3  $\mu\text{mol g}_{\text{Pt}}^{-1}\text{s}^{-1}$  can be achieved at 220 °C by photo-thermo catalysis, which is almost 4 times better than the best results reported for supported Pt catalysts (96.44  $\mu\text{mol g}_{\text{Pt}}^{-1}\text{s}^{-1}$ ) at the same reaction temperature,<sup>[11]</sup> even though the light intensity is only 250  $\text{mW cm}^{-2}$ .

To investigate how light and heat influence the reaction, the relationship between the reaction rates and the partial pressure of O<sub>2</sub> and C<sub>3</sub>H<sub>8</sub> were measured at 200 °C. It was found that the  $n$  value for O<sub>2</sub> is -1.4 in the absence of light (Figure 2a). The excessive O<sub>2</sub> in the reaction system would speed up the coverage and oxidation of Pt, leading to the degradation of the catalyst. That is, the oxygen can poison the surface of the supported Pt catalyst. However,  $n$  changes to 0.1 under light illumination, which means that the reaction

rate is almost independent of O<sub>2</sub> concentration under this condition. In the dark  $n$  is 0.9 for C<sub>3</sub>H<sub>8</sub> (Figure 2b), which is consistent with previous literature results.<sup>[12]</sup> It has been reported that activating the C-H bond of the hydrocarbon molecule is the kinetically relevant step (KRS) in the catalytic oxidation reaction, which occurs on the metallic Pt surface.<sup>[13]</sup> This high  $n$  value mainly originates from competitive absorption between O<sub>2</sub> and C<sub>3</sub>H<sub>8</sub>.<sup>[14]</sup> In contrast, the value of  $n$  for C<sub>3</sub>H<sub>8</sub> declines to 0.3 upon light illumination, suggesting that more C<sub>3</sub>H<sub>8</sub> molecules can reach the surface of metallic Pt and be activated. To examine the effect of the possible localized heat on the catalyst surface under light, the dependence of reaction rates on the partial pressure of O<sub>2</sub> and C<sub>3</sub>H<sub>8</sub> were further measured at 400 °C in the dark. The value of  $n$  for O<sub>2</sub> is increased to -0.6 in this case (Figure 2c), indicating that heating is beneficial for relieving the oxygen poisoning to some extent. Nevertheless, it is still difficult for C<sub>3</sub>H<sub>8</sub> molecules to approach the Pt surface since the value of  $n$  for C<sub>3</sub>H<sub>8</sub> is maintained at 0.9 (Figure 2d). The results unambiguously verify that photo-thermo catalysis is capable of accelerating the KRS of the oxidation reaction by suppressing the oxygen poisoning of the supported Pt catalyst and improving the accessibility of C<sub>3</sub>H<sub>8</sub> molecules.

To monitor the valence state of Pt in the photo-thermo reaction, in situ X-ray absorption spectroscopy (XAS) was conducted on the Pt/TiO<sub>2</sub>-WO<sub>3</sub> catalyst, in which the content of Pt was increased to 1 wt % and that of W to 4 wt % for an improved signal-to-noise ratio.<sup>[15]</sup> As shown in the normalized X-ray absorption near-edge structure (XANES) spectra

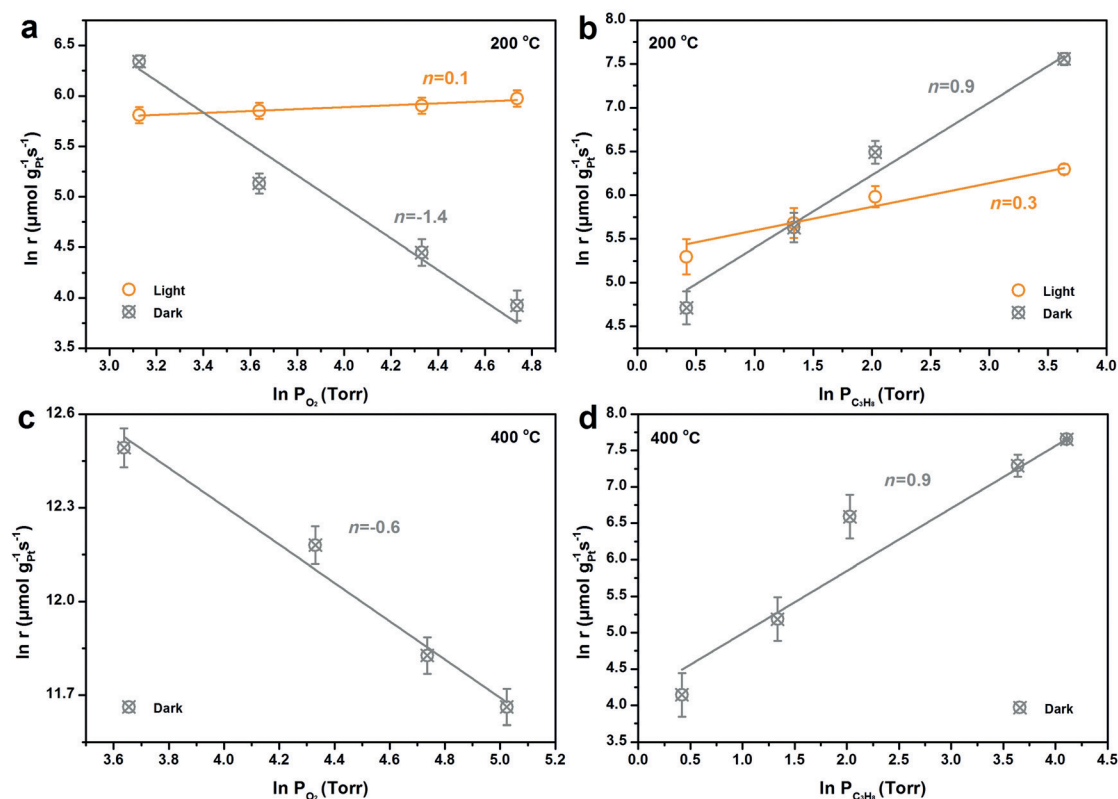


**Figure 2.** Dependence of reaction rate on partial pressure of a) O<sub>2</sub> and b) C<sub>3</sub>H<sub>8</sub> at 200 °C with and without light irradiation (power density: 500  $\text{mW cm}^{-2}$ ), as well as c) O<sub>2</sub> and d) C<sub>3</sub>H<sub>8</sub> at 400 °C in the dark.

(Figure 3a), the whiteline intensities of the activated and reacted catalysts are comparable, and slightly higher than that of the Pt foil but lower than those of the PtO<sub>2</sub> and Pt(NH<sub>3</sub>)<sub>4</sub>(NO<sub>3</sub>)<sub>2</sub> and calcined catalyst, suggesting that Pt is mainly in a metallic state during the continuous photo-thermo reaction (Figure S9). The metallic nature of the activated and reacted catalysts can also be verified by the dominant metallic Pt–Pt coordination in the extended X-ray absorption fine structure (EXAFS) spectra (Figure S10) and the corresponding fitting results (Table S2). In comparison with XAS, in situ DRIFTS of CO adsorption can afford firsthand information on the charges of Pt on the surface of the catalyst.<sup>[16]</sup> Figure 3b depicts the typical DRIFT spectra of CO chemisorbed on the Pt catalyst with and without light at 20 °C. When the light is turned off, there is a vibrational stretch at 2083 cm<sup>-1</sup> assigned to the oscillation of CO molecules linearly adsorbed on low-coordination metallic Pt,<sup>[17]</sup> in addition to the absorption bands of CO in the gas phase. Upon light illumination, a new band at 2093 cm<sup>-1</sup> appears accompanied by the decrease of the band at 2083 cm<sup>-1</sup>, suggesting that the surface of Pt is slightly electron deficient.<sup>[5]</sup> The photoinduced thermal effect can be excluded since heating would make the absorption band shift toward low wavenumbers (Figure S11). Therefore, this result demonstrates that the photoexcited electrons can be pumped from

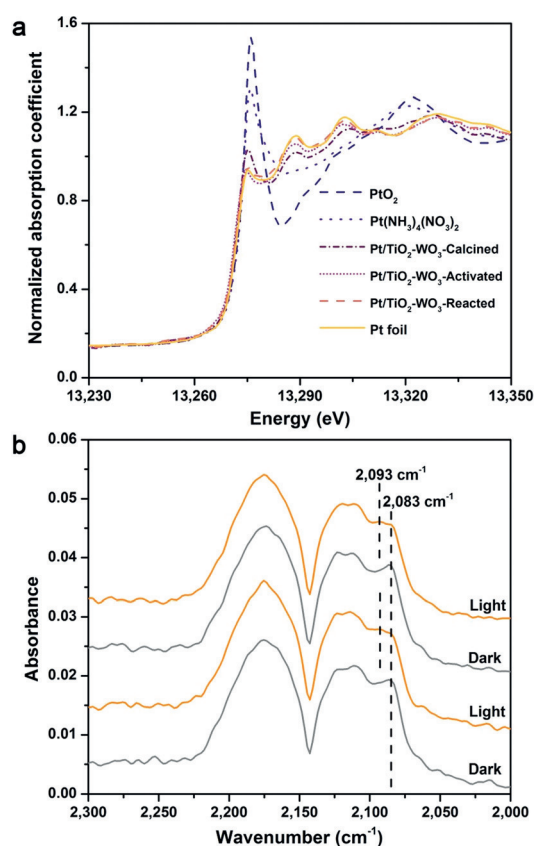


**Figure 3.** a) Normalized XANES spectra at the Pt L<sub>II</sub>-edge of PtO<sub>2</sub>, Pt(NH<sub>3</sub>)<sub>4</sub>(NO<sub>3</sub>)<sub>2</sub>, calcined Pt/TiO<sub>2</sub>-WO<sub>3</sub>, activated Pt/TiO<sub>2</sub>-WO<sub>3</sub>, reacted Pt/TiO<sub>2</sub>-WO<sub>3</sub>, and Pt foil. b) In situ DRIFTS of CO adsorbed on activated Pt/TiO<sub>2</sub>-WO<sub>3</sub> at 20 °C with and without light irradiation.

the 5d orbital of Pt to the vacant 2π\* orbital of CO by π-electron back donation under light, which is responsible for weakening the Pt–CO bond.<sup>[18]</sup> Furthermore, the phenomena are reversible with the light on and off, which indicates that the photoinduced electron could be produced reversibly. This is in good agreement with the catalytic result depicted in Figure 1d.

To capture the reaction intermediate, in situ DRIFTS of the catalyst in the reaction gas was performed. Figure S12a exhibits the evolution of the DRIFT spectra of the oxygenated carbonaceous species of C<sub>3</sub>H<sub>8</sub> oxidation in the dark. These bands remain unchanged with time. In contrast, a remarkable new band appears by introducing light illumination (red rectangle in Figure S12b). To identify the origin of the band, C<sub>3</sub>H<sub>8</sub> and O<sub>2</sub> were successively introduced into the sample cell under light. The DRIFT spectrum of the C<sub>3</sub>H<sub>8</sub> collected over the catalyst under light is identical to that of the C<sub>3</sub>H<sub>8</sub> gas phase (Figure 4a).<sup>[19]</sup> This indicates that the interaction between C<sub>3</sub>H<sub>8</sub> and the catalyst is weak, and it excludes the possibility of direct activation of C<sub>3</sub>H<sub>8</sub> molecules and confirms the participation of O<sub>2</sub> in forming the new species. Concurrent with the reduction of the IR features of

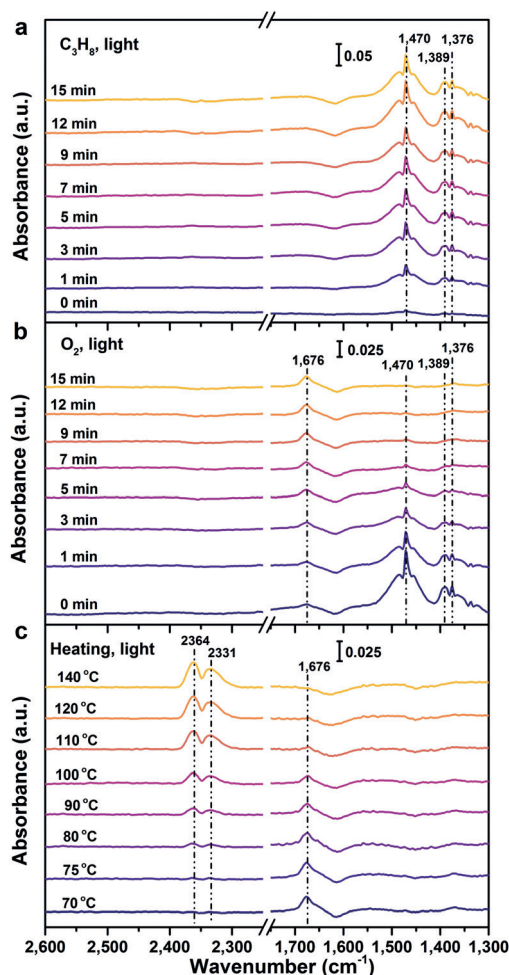


**Figure 4.** In situ DRIFT spectra of the Pt/TiO<sub>2</sub>-WO<sub>3</sub> catalyst successively contacted with a) C<sub>3</sub>H<sub>8</sub>, b) O<sub>2</sub> at 70 °C under light illumination, and c) heated to different temperatures.

$C_3H_8$ , a band at  $1676\text{ cm}^{-1}$  grows in the time-resolved DRIFT spectra in the presence of  $O_2$  (Figure 4b). This newly generated principal band is ascribed to the stretching vibration of peroxy carbonate (compare to the  $-OCO_3$  band at  $1678\text{ cm}^{-1}$  for  $(Ph_3P)_2PtOCO_3$ ).<sup>[20]</sup> When the temperature is raised, the decomposition of peroxy carbonate can be accelerated, which is evidenced by an increase of the bands of gaseous  $CO_2$  at  $2331\text{ cm}^{-1}$  and  $2364\text{ cm}^{-1}$  (Figure 4c). This result confirms that peroxy carbonate is the intermediate of the photo-thermo catalytic oxidation of  $C_3H_8$ . Using density functional theory (DFT), peroxy carbonate has been verified as the reaction intermediate in CO oxidation on supported Pt clusters.<sup>[21]</sup>

The significant change in the reaction order  $n$  of  $O_2$  under light irradiation suggests that the photo-thermo reaction follows a very distinct pathway in which light induces the evolution of oxygen species to drive the reaction. Therefore, identifying active oxygen species is crucial for understanding the underlying mechanism. To this end, EPR was employed, which is a robust technique for detecting unpaired electrons.<sup>[22]</sup> Figure 5a presents the in situ EPR spectra obtained at 100 K in air on the reduced  $Pt/TiO_2-WO_3$  catalyst, with and without light illumination. In the dark, the symmetric signal at  $g = 2.003$  is a consequence of unpaired electrons trapped at the oxygen vacancies in  $TiO_2$ ,<sup>[23]</sup> and the prominent signal at  $g = 1.979$  is attributed to  $Ti^{3+}$  in the rutile lattice of Degussa P25.<sup>[24]</sup> Upon continuous illumination for 5 minutes, a set of paramagnetic superoxide anion  $O_2^-$  ( $g_{xx} = 2.002$ ,  $g_{yy} = 2.010$ ,  $g_{zz} = 2.026$ ) signals were observed on the reduced  $Pt/TiO_2-WO_3$  catalyst.<sup>[25]</sup> Meanwhile, the EPR signals of  $O_2^-$  weaken considerably under light once  $C_3H_8$  is introduced, signifying

that  $O_2^-$  can react with  $C_3H_8$  even at 100 K (Figure 5b). This process is reversible with and without light illumination, further confirming the importance of photoinduced  $O_2^-$  in this reaction.

The role of  $WO_3$  in our catalyst can also be clarified by EPR measurements. Distinct from reduced  $Pt/TiO_2-WO_3$ , EPR signals from reduced  $Pt/TiO_2$  were seen at  $g = 2.026$ ,  $2.017$ , and  $2.014$  (Figure S13), which are assigned to  $O_2^-$ ,  $O_3^-$ , and  $O^-$ , respectively.<sup>[26]</sup> Compared with  $Pt/TiO_2$ , the exclusive oxygen intermediate ( $O_2^-$ ) produced on the  $Pt/TiO_2-WO_3$  catalyst should be responsible for its high activity (Figure S14). Furthermore, a sharp signal at  $g = 1.990$  responsible for  $Ti^{3+}$  in the anatase lattice appears over the reduced  $Pt/TiO_2$  under light,<sup>[55]</sup> in parallel with the increase of the signal intensity of  $Ti^{3+}$  in the rutile lattice. In this regard, it can be interpreted that excess photogenerated electrons induce the reduction of  $Ti^{4+}$  in the Degussa P25 lattice.<sup>[26a]</sup> The absence of  $Ti^{3+}$ ,  $O^-$ , and  $O_3^-$  over  $Pt/TiO_2-WO_3$  give evidence for electron transfer from  $TiO_2$  to  $WO_3$  arising from proper band alignment. To validate this assumption, photoluminescence (PL) spectra were collected to compare charge separation ability (Figure S15). Evidently, the addition of  $WO_3$  can substantially reduce the PL intensity of  $TiO_2$ , indicating suppressed charge recombination. Moreover, the participation of  $WO_3$  increases the utilization of irradiated light on the support (Figure S1).

The origin of the photogenerated electrons was studied by comparing the catalytic activities of the  $Pt/Al_2O_3$  with and without light irradiation (Figure S16). Compared with the  $Pt/TiO_2-WO_3$  catalyst (Figure 1a), the catalytic performance of the  $Pt/Al_2O_3$  catalyst under light is slightly better than that in the dark, for which the direct photoexcitation of hybridized  $Pt-O_2$  states may be responsible.<sup>[27]</sup> Moreover, the light absorption of  $Pt/TiO_2-WO_3$  is similar to that of  $TiO_2-WO_3$  (Figure S17). The aforementioned results indicate that there is no plasmonic effect over the Pt clusters.<sup>[5]</sup> Therefore, the electronic effect should be from the  $TiO_2-WO_3$  support. To further verify the contributions of the charge carriers, potassium dichromate and ammonium oxalate are used as electron and hole scavengers, respectively.<sup>[28]</sup> The conversion of  $C_3H_8$  is approximately 77% when the catalyst was ground with inert quartz sand. The trapping of electrons and holes result in a decrease of the equilibrium conversion of  $C_3H_8$  (Figure 6a). These results indicate that the trapping of holes or electrons inhibit the reaction. To understand the activation and desorption of oxygen on the catalyst, temperature-programmed desorption of  $O_2$  ( $O_2$ -TPD) was conducted. No  $O_2$  moieties were detected when the  $O_2$  adsorption process was conducted under light (Figure 6b), indicating that light illumination restrains  $O_2$  adsorption on the catalyst. Two prominent peaks appear at around  $188^\circ\text{C}$  and  $294^\circ\text{C}$  in the dark, which correspond to different kinds of chemically adsorbed  $O_2^*$  species.<sup>[29]</sup> In sharp contrast,  $O_2^*$  species begin to desorb at room temperature and attain a summit at  $105^\circ\text{C}$  under light. The baseline drifts downward upon illumination at the beginning, which may stem from the consumption of physically adsorbed  $O_2$ . These results suggest that light illumination is helpful for the activation and desorption of oxygen species.

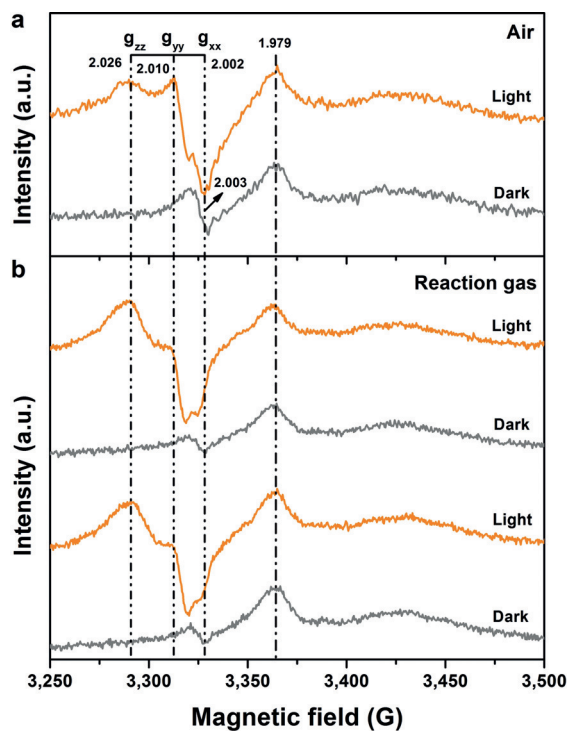


**Figure 5.** In situ EPR spectra of the reduced  $Pt/TiO_2-WO_3$  catalyst a) in air and b) in reaction gas with and without light irradiation.

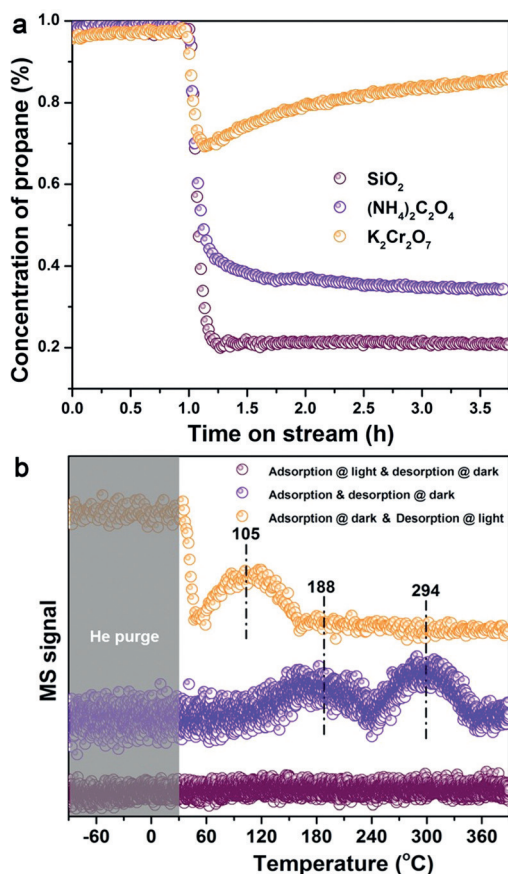


**Figure 6.** a) Catalytic activity of the Pt/TiO<sub>2</sub>-WO<sub>3</sub> catalyst mixed with SiO<sub>2</sub>, (NH<sub>4</sub>)<sub>2</sub>C<sub>2</sub>O<sub>4</sub>, and K<sub>2</sub>Cr<sub>2</sub>O<sub>7</sub> under light illumination. b) O<sub>2</sub>-TPD profiles of the Pt/TiO<sub>2</sub>-WO<sub>3</sub> catalyst under different conditions.

Based on our results, the corresponding mechanisms are proposed. For thermocatalysis, O<sub>2</sub> would preferentially adsorb onto the surface of the active Pt cluster because of higher affinity, resulting in oxygen poisoning (Figure 7a). A higher temperature imbues the adsorbed oxygen species with

high activity, thereby driving the catalytic oxidation reaction. However, the excess O<sub>2</sub> suffers from competitive adsorption with hydrocarbons and also oxidizes the metallic Pt, which leads to the low performance of the catalyst.<sup>[8a]</sup> Photo-thermo catalysis over the Pt/TiO<sub>2</sub>-WO<sub>3</sub> catalyst brings about a great change (Figure 7b). The O<sub>2</sub> adsorbed onto the Pt surface can be activated to generate anionic superoxide (Pt-O-O<sup>δ-</sup>) by photogenerated electrons from the semiconductors (in situ EPR results in Figure 5a). The active O<sub>2</sub><sup>-</sup> species would readily desorb (O<sub>2</sub>-TPD results in Figure 6b) and react with the adjacently activated C<sub>3</sub>H<sub>8</sub><sup>\*</sup> to produce carbonate (in situ EPR results in Figure 5b), followed by the formation of peroxy carbonate with the mediation of holes<sup>[30]</sup> (in situ DRIFT results in Figures 4a,b). Subsequently, the decomposition of the peroxy carbonate can be accelerated by heating to produce gaseous CO<sub>2</sub> (in situ DRIFT results in Figure 4c) and chemisorbed O<sub>2</sub><sup>\*</sup>. The E<sub>a</sub> can be reduced considerably by the above steps. For improving the reaction rate, suitable heating is of the essence in photo-thermo catalysis. The conductivity of semiconductors increases exponentially with the temperature.<sup>[31]</sup> We can infer that the elevated temperature may be conducive to transfer of more energetic charge carriers to the active sites of the catalyst. From the thermal catalytic point of view, heating would also profit the desorption and/or transform of the intermediates on the catalyst. Thus, the synergy between photocatalysis and thermocatalysis are exemplified.

## Conclusion

In summary, photo-thermo catalysis has been demonstrated to be an effective strategy for promoting catalytic oxidation reactivity over the semiconductor-supported non-plasmonic metal Pt—especially at low reaction temperatures. The inversely linear dependence of the apparent activation energy on the intensity of light, and the great change of the reaction orders, unravel the essence of the advantages for the photo-thermo catalytic oxidation reaction, in which overcoming the oxygen poisoning of the supported Pt catalyst is

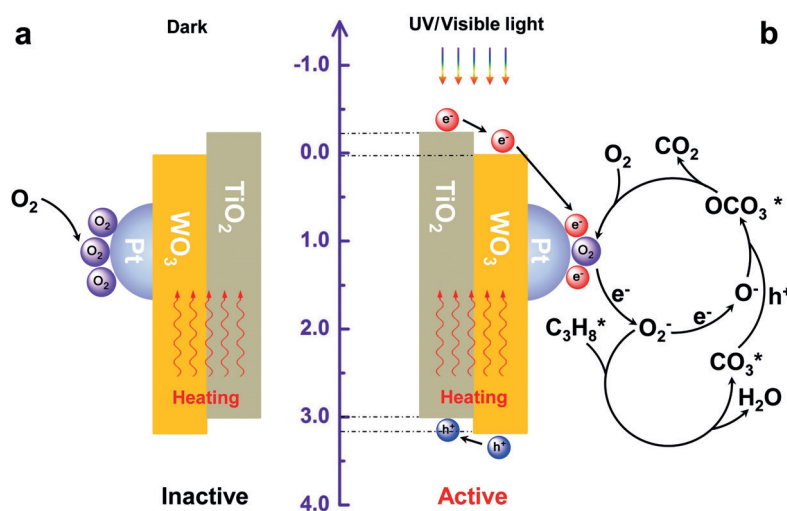


**Figure 7.** Proposed reaction mechanisms of a) thermal and b) photo-thermo oxidation of C<sub>3</sub>H<sub>8</sub> over the Pt/TiO<sub>2</sub>-WO<sub>3</sub> catalyst at low temperatures.

the key factor to accelerate the activation of C–H on the Pt surface. The roles of the nonplasmonic metal Pt and the semiconductor support in the catalytic photo–thermo oxidation process are clarified: the decreased electron density of Pt could enhance the activation of oxygen, while the TiO<sub>2</sub>–WO<sub>3</sub> support promotes the utilization of light and suppresses charge recombination. Combined with the carbonaceous intermediate and active oxygen species detected by in situ characterizations, a new reaction route for photo–thermo catalysis at low temperatures is proposed, which provides in-depth insight into the photo–thermo catalysis of semiconductor-supported nonplasmonic metal catalysts.

## Acknowledgements

We are grateful for support from the National Key R&D Program of China (2016YFA0202801), the Strategic Priority Research Program of the Chinese Academy of Sciences (XDB17020400), the National Natural Science Foundation of China (21776271, CSC 201804910082), CAS Interdisciplinary Innovation Team (BK2018001) and the China Postdoctoral Science Foundation (2017M621171). We also thank the BL 14W beamline at the Shanghai Synchrotron Radiation Facility (SSRF). A.I.F. acknowledges support by the U.S. Department of Energy, Office of Basic Energy Sciences under Grant No. DE-FG02-03ER15476, and by the Laboratory Directed Research and Development Program through LDRD 20-040 of Brookhaven National Laboratory under U.S. Department of Energy Contract No. DE-SC0012704.

## Conflict of interest

The authors declare no conflict of interest.

**Stichwörter:** oxygen poisoning · photocatalysis · Pt catalysts · reaction order · semiconductors

- [1] Z. Wang, H. Song, H. Liu, J. Ye, *Angew. Chem. Int. Ed.* **2020**, *59*, 8016–8035; *Angew. Chem.* **2020**, *132*, 8092–8111.
- [2] a) Z. Li, J. Liu, Y. Zhao, G. I. N. Waterhouse, G. Chen, R. Shi, X. Zhang, X. Liu, Y. Wei, X. D. Wen, L. Z. Wu, C. H. Tung, T. Zhang, *Adv. Mater.* **2018**, *30*, 1800527; b) F. Liu, M. Zeng, Y. Li, Y. Yang, M. Mao, X. Zhao, *Adv. Funct. Mater.* **2016**, *26*, 4518–4526; c) X. Meng, T. Wang, L. Liu, S. Ouyang, P. Li, H. Hu, T. Kako, H. Iwai, A. Tanaka, J. Ye, *Angew. Chem. Int. Ed.* **2014**, *53*, 11478–11482; *Angew. Chem.* **2014**, *126*, 11662–11666; d) W. Gao, R. Gao, Y. Zhao, M. Peng, C. Song, M. Li, S. Li, J. Liu, W. Li, Y. Deng, *Chem* **2018**, *4*, 2917–2928.
- [3] a) P. Christopher, H. Xin, A. Marimuthu, S. Linic, *Nat. Mater.* **2012**, *11*, 1044–1050; b) T. H. Tan, J. Scott, Y. H. Ng, R. A. Taylor, K. F. Aguey-Zinsou, R. Amal, *ACS Catal.* **2016**, *6*, 1870–1879; c) C. H. Hao, X. N. Guo, Y. T. Pan, S. Chen, Z. F. Jiao, H. Yang, X. Y. Guo, *J. Am. Chem. Soc.* **2016**, *138*, 9361–9364; d) L. Zhou, D. F. Swearer, C. Zhang, H. Robotjazi, H. Zhao, L. Henderson, L. Dong, P. Christopher, E. A. Carter, P. Nordlander, N. J. Halas, *Science* **2018**, *362*, 69–72; e) X. Guo, C. Hao, G. Jin, H. Zhu, X. Guo, *Angew. Chem. Int. Ed.* **2014**, *53*, 1973–1977; *Angew. Chem.* **2014**, *126*, 2004–2008.
- [4] a) B. Zhao, Y. Jian, Z. Jiang, R. Albilali, C. He, *Chin. J. Catal.* **2019**, *40*, 543–552; b) T. Cai, J. Yuan, L. Zhang, L. Yang, Q. Tong, M. Ge, B. Xiao, X. Zhang, K. Zhao, D. He, *Catal. Sci. Technol.* **2018**, *8*, 5416.
- [5] Y. Zhou, D. E. Doronkin, Z. Zhao, P. N. Plessow, J. Jelic, B. Detlefs, T. Pruessmann, F. Studt, J. D. Grunwaldt, *ACS Catal.* **2018**, *8*, 11398–11406.
- [6] a) B. Y. Xia, H. B. Wu, X. Wang, X. W. Lou, *J. Am. Chem. Soc.* **2012**, *134*, 13934–13937; b) Y. Xu, A. V. Ruban, M. Mavrikakis, *J. Am. Chem. Soc.* **2004**, *126*, 4717–4725.
- [7] a) Y. H. Chin, C. Buda, M. Neurock, E. Iglesia, *J. Am. Chem. Soc.* **2011**, *133*, 15958–15978; b) M. García-Diéguez, Y. H. Chin, E. Iglesia, *J. Catal.* **2012**, *285*, 260–272.
- [8] a) C. P. O'Brien, G. R. Jenness, H. Dong, D. G. Vlachos, I. C. Lee, *J. Catal.* **2016**, *337*, 122–132; b) W. Tang, W. Xiao, S. Wang, Z. Ren, J. Ding, P. X. Gao, *Appl. Catal. B* **2018**, *226*, 585–595.
- [9] a) J. G. Santiesteban, D. C. Calabro, W. S. Borghard, C. D. Chang, J. C. Vartuli, Y. P. Tsao, M. A. Natal-Santiago, R. D. Bastian, *J. Catal.* **1999**, *183*, 314–322; b) N. Lei, X. Zhao, B. Hou, M. Yang, M. Zhou, F. Liu, A. Wang, T. Zhang, *ChemCatChem* **2019**, *11*, 3903–3912.
- [10] H. Yoshida, Y. Yazawa, T. Hattori, *Catal. Today* **2003**, *87*, 19–28.
- [11] a) H. Luo, X.-D. Wu, D. Weng, S. Liu, R. Ran, *Rare Met.* **2017**, *36*, 1–9; b) Y. R. Liu, X. Li, W. M. Liao, A. P. Jia, Y. J. Wang, M. F. Luo, J. Q. Lu, *ACS Catal.* **2019**, *9*, 1472–1481.
- [12] T. F. Garetto, E. Rincon, C. R. Apesteguia, *Appl. Catal. B* **2004**, *48*, 167–174.
- [13] R. Burch, M. J. Hayes, *J. Mol. Catal. A* **1995**, *100*, 13–33.
- [14] Y. Yazawa, H. Yoshida, T. Hattori, *Appl. Catal. A* **2002**, *237*, 139–148.
- [15] a) X. Liu, M. H. Liu, Y. C. Luo, C. Y. Mou, S. D. Lin, H. Cheng, J. M. Chen, J. F. Lee, T. S. Lin, *J. Am. Chem. Soc.* **2012**, *134*, 10251–10258; b) Y. Tan, X. Y. Liu, L. Zhang, A. Wang, L. Li, X. Pan, S. Miao, M. Haruta, H. Wei, H. Wang, F. Wang, X. Wang, T. Zhang, *Angew. Chem. Int. Ed.* **2017**, *56*, 2709–2713; *Angew. Chem.* **2017**, *129*, 2753–2757.
- [16] B. Qiao, A. Wang, X. Yang, L. F. Allard, Z. Jiang, Y. Cui, J. Liu, J. Li, T. Zhang, *Nat. Chem.* **2011**, *3*, 634–641.
- [17] L. DeRita, S. Dai, K. Lopez-Zepeda, N. Pham, G. W. Graham, X. Pan, P. Christopher, *J. Am. Chem. Soc.* **2017**, *139*, 14150–14165.
- [18] K. C. Chou, S. Westerberg, Y. R. Shen, P. N. Ross, G. A. Somorjai, *Phys. Rev. B* **2004**, *69*, 153413.
- [19] M. A. Hasan, M. I. Zaki, L. Pasupulety, *J. Phys. Chem. B* **2002**, *106*, 12747–12756.
- [20] P. Hayward, D. Blake, G. Wilkinson, C. Nyman, *J. Am. Chem. Soc.* **1970**, *92*, 5873–5878.
- [21] A. D. Allian, K. Takanebe, K. L. Fuldala, X. Hao, T. J. Truex, J. Cai, C. Buda, M. Neurock, E. Iglesia, *J. Am. Chem. Soc.* **2011**, *133*, 4498–4517.
- [22] H. C. Chang, B. Mondal, H. Fang, F. Neese, E. Bill, S. Ye, *J. Am. Chem. Soc.* **2019**, *141*, 2421–2434.
- [23] H. Guan, J. Lin, B. Qiao, X. Yang, L. Li, S. Miao, J. Liu, A. Wang, X. Wang, T. Zhang, *Angew. Chem. Int. Ed.* **2016**, *55*, 2820–2824; *Angew. Chem.* **2016**, *128*, 2870–2874.
- [24] N. Siemer, A. Luken, M. Zalibera, J. Frenzel, D. Munoz-Santiburcio, A. Savitsky, W. Lubitz, M. Muhler, D. Marx, J. Strunk, *J. Am. Chem. Soc.* **2018**, *140*, 18082–18092.
- [25] H. Sakamoto, T. Ohara, N. Yasumoto, Y. Shiraishi, S. Ichikawa, S. Tanaka, T. Hirai, *J. Am. Chem. Soc.* **2015**, *137*, 9324–9332.
- [26] a) N. Siedl, S. O. Baumann, M. J. Elser, O. Diwald, *J. Phys. Chem. C* **2012**, *116*, 22967–22973; b) I. Caretti, M. Keulemans, S. W. Verbruggen, S. Lenaerts, S. Van Doorslaer, *Top. Catal.* **2015**, *58*, 776–782.
- [27] M. J. Kale, T. Avanesian, H. Xin, J. Yan, P. Christopher, *Nano Lett.* **2014**, *14*, 5405–5412.

- [28] R. Zhang, H. Wang, S. Tang, C. Liu, F. Dong, H. Yue, B. Liang, *ACS Catal.* **2018**, 8, 9280–9286.
- [29] J. J. Li, S. C. Cai, E. Q. Yu, B. Weng, X. Chen, J. Chen, H. P. Jia, Y. J. Xu, *Appl. Catal. B* **2018**, 233, 260–271.
- [30] H. Arakawa, K. Sayama, *Catal. Surv. Jpn.* **2000**, 4, 75–80.
- [31] W. D. Callister, D. G. Rethwisch, *Materials science and engineering: An introduction*, Wiley, New York, **2007**.

Manuskript erhalten: 2. Februar 2020  
Veränderte Fassung erhalten: 18. März 2020  
Akzeptierte Fassung online: 5. April 2020  
Endgültige Fassung online: 29. Mai 2020

---